Impedance Profile Prediction for Grid-Connected VSCs based on Feature Extraction

Yang Wu*, Heng Wu*, Li Cheng†, Jianyu Zhou†, Zichao Zhou†, Minjie Chen‡ and Xiongfei Wang†*

*Department of Energy, Aalborg Univeristy, Aalborg, Denmark

† Division of Electric Power and Energy Systems, KTH Royal Institute of Technology, Stockholm, Sweden

‡ Department of Electrical and Computer Engineering, Princeton University, Princeton NJ, USA

Email: *{yawu, hew}@energy.aau.dk, †{lichengphd, jizhou, zichaoz, xiongfei}@kth.se, tminjie@princeton.edu

Abstract—Impedance-based stability analysis has been widely adopted for voltage source converters (VSCs). Considering unknown controller parameters, impedance measurement based on frequency scan is always required for stability evaluation, which endures complicated implementation and can only be conducted under small amount of stable operating conditions. To solve this problem, a novel impedance profile prediction method for grid-connected VSCs has been proposed. A combined structure of stacked autoencoder (AE) and principal component analysis (PCA) is firstly proposed to extract VSC admittance feature under stable operating points, and a comprehensive VSC admittance set can be further predicted through searching on an enlarged feature space with unstable scenarios included. The stability can then be evaluated on the predicted VSC admittances with a stability boundary derived. Simulations and experiments prove the effectiveness of the proposed method.

Keywords—Voltage source converter, impedance-based stability analysis, machine learning.

I. INTRODUCTION

Large-scale integration of renewable energy will appear in future power grids with power electronic converters as interfaces. However, the interaction of power converters and grid may lead to resonance in a wide frequency range, influencing system stability [1], [2]. Therefore, the stability of grid-connected VSCs is essential for safe system operation.

Stability issue of grid-connected VSCs has been studied for decades, and most existing methods can be classified into state-space-based approach in time domain or impedance-based approach in frequency domain [3]. The state-space-based approach establishes the complete state-space equation for the controller and power stage of the converter, and system stability can then be evaluated by calculating the eigenvalues of the state matrix [4]. The sensitivity of different controller parameters can also be obtained by inspecting the damping ratio. However, such methods require detailed information of the controller structure and parameters, which is hard to be obtained in industry practices due to intellectual property (IP) protection from different vendors [5], [6].

Frequency-domain analysis provides a feasible way to solve this issue, which can be realized based on generalized Nyquist criterion (GNC) and VSC impedance measurement by frequency scan [7]-[10]. However, the impedance

This work was supported by the European Union's Horizon 2020 Research and Innovation Programme under the Marie Skłodowska-Curie Grant Agreement 101107634 (PhyDAWN).

measurement can only by conducted under limited amount of stable operating points, which fails to predict other possible impedance profiles. Furthermore, online impedance measurement can be time-consuming and hard to implement [11]. Some recent researches have proposed estimating the relationship between the VSC terminal admittance and operating points by curve fitting algorithms [12]. However, prior knowledge of the controller structure is still needed and the estimation accuracy on a wide frequency range is limited.

To solve this problem, this paper proposes a novel impedance profile prediction method for grid-connected VSCs with unknown controller configurations, which is able to predict unstable cases and draw stability boundary solely using small amount of stable operating data. Based on the proposed method, stability evaluation for grid-connected VSCs can be simplified by measuring the admittance at single or certain frequencies, and is more convenient to apply in the industry.

II. IMPEDANCE PROFILE OF GRID-CONNECTED VSCs

A. System Configuration

In this paper, a typical three-phase grid-connected VSC is taken as an example. The system configuration and control diagram are shown in Fig. 1. A synchronous reference frame phase-locked loop (SRF-PLL) is used to synchronize the VSC with the grid, and the converter is regulated as a constant power source by cascaded power controller and current controller. Voltage feedforward control is also used for transient performance enhancement by adding the PCC voltage on the output of the current controller. L_f represents the filter inductor, while L_g represents the grid inductance.

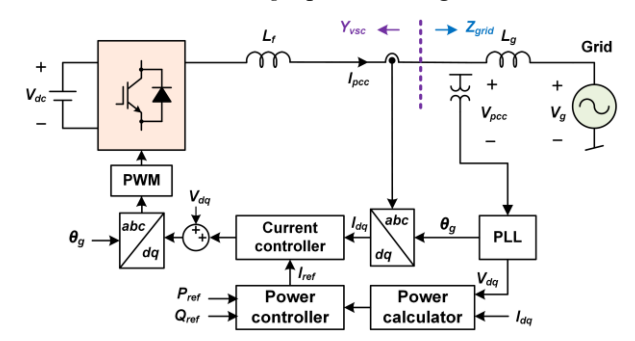
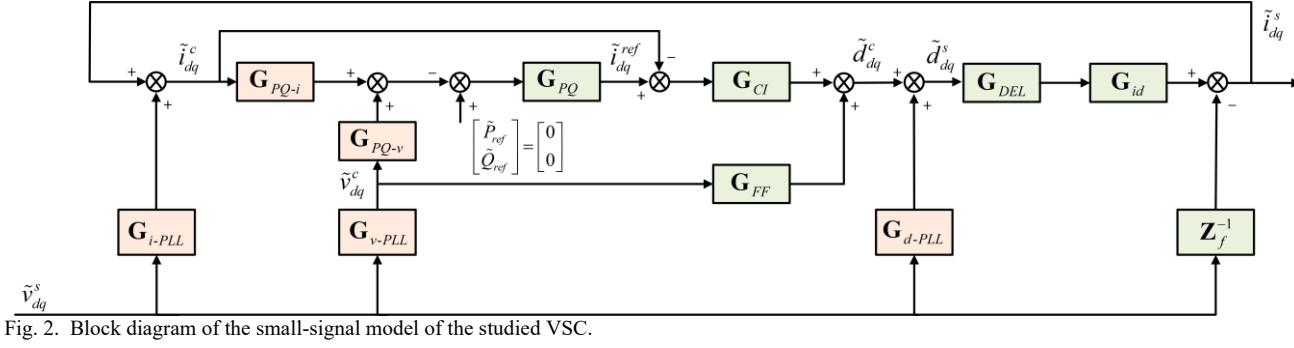


Fig. 1. System configuration and control diagram of the studied grid-connected VSC system.

B. Impedance Profile Generation for Grid-Connected VSCs

For the convenience of stability analysis, the VSC admittance Y_{VSC} in dq-frame is used to evaluate the stability



$$\mathbf{Y}_{VSC} = -\left(\mathbf{I} + \mathbf{G}_{id}\mathbf{G}_{DEL}\mathbf{G}_{CI}\right)^{-1}\left(\mathbf{Z}_{f}^{-1} + \mathbf{G}_{id}\mathbf{G}_{DEL}\left(\mathbf{G}_{d-PLL} + \mathbf{G}_{FF}\mathbf{G}_{v-PLL} + \mathbf{G}_{CI}\left(\mathbf{G}_{PQ}\mathbf{G}_{PQ-v}\mathbf{G}_{v-PLL} - \mathbf{G}_{i-PLL}\right)\right)\right)$$
(1)

of the entire system, which can be derived based on the small-signal modeling theory [7]. The block diagram of the small-signal model is shown in Fig. 2, where \mathbf{G}_{PQ-i} and \mathbf{G}_{PQ-v} represent the linearization matrix in power calculation. G_{PO} and G_{CI} represents the PI controller for the power control and current control, respectively. G_{FF} is an identity matrix representing the feedforward control. G_{DEL} denotes the digital delay of the controller. G_{id} represents the transfer function matrix between the output of the converter and the output current, and \mathbf{Z}_f represents the impedance matrix of the filter inductance. $\mathbf{G}_{i\text{-PLL}}$, $\mathbf{G}_{v\text{-PLL}}$ and $\mathbf{G}_{d\text{-PLL}}$ denote the influence of PLL on the current, voltage and duty ratio when transformed between system dq-frame and controller dqframe. According to Fig. 2, the VSC terminal admittance \mathbf{Y}_{VSC} can be derived as (1), where I represents identity matrix.

Especially, the linearization matrix for power calculation and the transformation matrices related to PLL can be expressed as (2)-(6), where V_{pcc} represents the steady-state voltage aligned to d-axis. I_{d0} and I_{q0} represent the steady-state current of dq-axis, respectively. G_{PLL} represents the transfer function of the SRF-PLL, which can be expressed as (7). K_p PLL and K_{i-PLL} represent the proportional and integral gain of the PLL. The rest of the transfer function matrices in the block diagram have been included in the Appendix A.

$$\mathbf{G}_{PQ-i} = \begin{bmatrix} V_{pcc} & 0\\ 0 & -V_{pcc} \end{bmatrix} \tag{2}$$

$$\mathbf{G}_{PQ-v} = \begin{bmatrix} I_{d0} & I_{q0} \\ -I_{q0} & I_{d0} \end{bmatrix}$$
 (3)

$$\mathbf{G}_{i\text{-}PLL} = \begin{bmatrix} 0 & I_{q0}G_{PLL} \\ 0 & -I_{d0}G_{PLL} \end{bmatrix}$$
 (4)

$$\mathbf{G}_{v-PLL} = \begin{bmatrix} 1 & 0 \\ 0 & 1 - V_{pcc} G_{PLL} \end{bmatrix}$$
 (5)

$$\mathbf{G}_{d\text{-}PLL} = \begin{bmatrix} 0 & -D_{q0}G_{PLL} \\ 0 & D_{d0}G_{PLL} \end{bmatrix}$$
 (6)

$$G_{PLL} = \frac{K_{p-PLL} + K_{i-PLL} / S}{s + V_{pcc} \left(K_{p-PLL} + K_{i-PLL} / S\right)}$$
(7)

It can be observed that the above matrices are all related to the operating point, making the terminal impedance profile \mathbf{Y}_{VSC} also closely related to the operating point. However, measuring the impedance at a large amount of operating points is time-consuming and hard to achieve in practices. Furthermore, traversing the entire set of possible operating points cannot be achieved. Therefore, prediction of VSC admittance set based on limited amount of terminal admittance measurement data becomes highly desirable in the industry.

III. VSC ADMITTANCE PREDICTION BASED ON STACKED-AUTOENCODER AND PCA

To predict comprehensive VSC admittance set based on measurements at small amount of stable operating points, a novel prediction method based on stacked autoencoder (AE) has been proposed in this paper, whose structure is shown in Fig. 3. As the VSC admittance profiles differ due to the variation of V_{pcc} , I_{d0} and I_{q0} , it will be possible to represent every admittance profile by no more than 3 variables. Considering unknown controller parameters, features extracted by stacked AE are used to represent the admittance profiles, instead of normal operating points. The stacked AE can be regarded as a special feedforward neural network (NN) with multiple hidden layers [13]. Unlike traditional NNs, the inputs and outputs of the stacked AE are kept the same in the training process, which are the VSC admittances. Therefore, by keeping the neuron numbers in the middlehidden layer (feature layer) as small as possible while ensuring an acceptable error for the outputs, the neurons in the feature layer will be able to represent different admittance profiles, forming a latent mapping to the operating points.

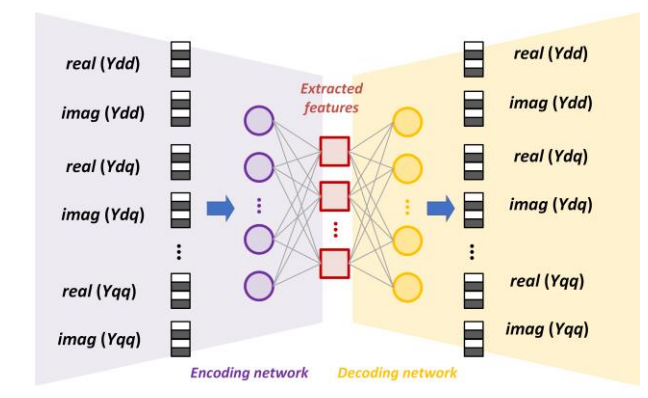


Fig. 3. Structure of the stacked AE.

The loss function for the training of the stacked AE is defined as (8), where N_s is the sample number of the dataset and N_f is the number of the studied frequencies. Y_{dd} (OP_i, f_j) represents Y_{dd} at the ith operating point and jth frequency, whose corresponding reconstructed value by the stacked AE is represented by Y_{dd-i} (f_j). Similar expressions are also adopted for Y_{dq} , Y_{qd} and Y_{qq} .

$$Loss = \sum_{i=1}^{N_{s}} \sum_{j=1}^{N_{f}} \left(real\left(Y_{dd}\left(OP_{i}, f_{j}\right)\right) - real\left(Y_{dd-i}\left(f_{j}\right)\right) \right)^{2} + \left(imag\left(Y_{dd}\left(OP_{i}, f_{j}\right)\right) - imag\left(Y_{dd-i}\left(f_{j}\right)\right) \right)^{2} + K + \left(imag\left(Y_{qq}\left(OP_{i}, f_{j}\right)\right) - imag\left(Y_{qq-i}\left(f_{j}\right)\right) \right)^{2} \right)$$

$$(8)$$

To validate the effectiveness of the proposed method, a dataset composed of 720 VSC admittances under stable operating points is generated based on the analytical smallsignal VSC model derived in Section II. The used parameters of the VSC are listed in the Appendix B. The grid inductance L_g is set as 6 mH, ensuring that all the studied cases are in stable operation. The selected operating points are as follows: V_{pcc} ranges in [99 V, 121 V], I_{d0} ranges in [-6 A, 6 A], and I_{q0} ranges in [-2 A, 2 A]. The entire dataset is then divided into training set, validation set and test set in a 70%:15%:15% portion. The training for feature extraction of the stacked AE is conducted with hyper-parameters selected as Table I. It is found that a neuron number of 2 in the feature layer is enough for the admittance reconstruction, which also stands for the feature number used in the following analysis. The performance of the AE can then be validated on the test set. A randomly selected sample from the test set is shown in Fig. 4, proving the effectiveness of using features to reconstruct the VSC admittance.

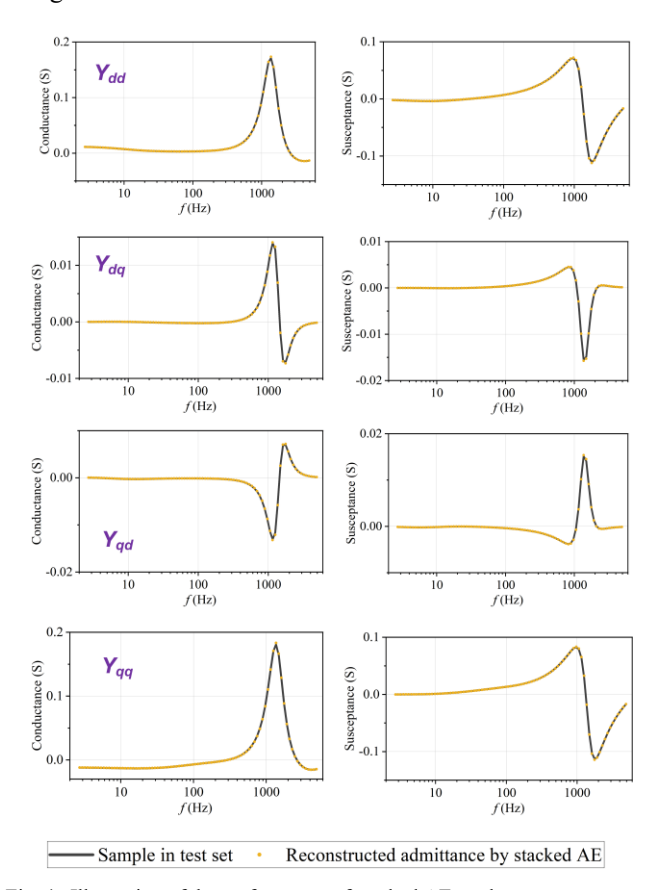


Fig. 4. Illustration of the performance of stacked AE on the test set.

The mean absolute error (MAE) is used for the evaluation of the stacked AE. The MAE on the training set and the test set are calculated to be 3.06×10^{-4} S and 3.16×10^{-4} S, proving the accuracy of the reconstructed admittance by the trained stacked AE.

TABLE I - HYPER-PARAMETERS OF THE STACKED AE

Optimizer	Adam (TensorFlow)	
Neuron numbers in each layer	712, 32, 2 (feature number), 32, 712	
Hidden-layer activation function	linear	
Output-layer activation function	activation function linear	
Learning rate	0.012	
Decay steps 50		
Decay rate	0.98	
Epoch number 1000		

Furthermore, a generalization test set has been considered, which includes VSC admittances with I_{d0} ranging in [-18 A, 18 A] and I_{q0} ranging in [-5 A, 5 A]. It should be noted that many unstable operating scenarios have been included now. The MAE on this new test set is calculated to be 4.97×10^{-4} S, proving that the extracted features can also represent VSC admittance profiles for unstable operating scenarios which have not been trained. Therefore, thorough searching on the feature space for additional VSC admittance generation becomes feasible.

The feature distribution on the training set is then studied, as shown in Fig.5(a). It is shown that the feature values present an uneven distribution, indicating that they are not totally decoupled. For more effective generation of possible VSC admittances, principal component analysis (PCA) is adopted to orthogonalize the feature space [14]. The feature distribution after PCA is shown in Fig. 5(b), which now distribute evenly for convenient VSC admittance generation.

Color scale based on the value of Feature 1

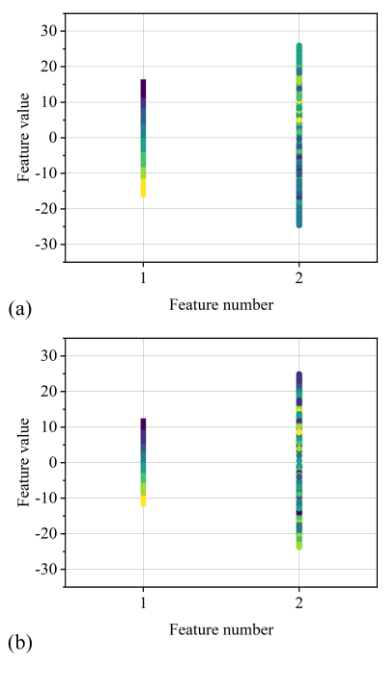


Fig. 5. (a) The distribution of extracted features by the stacked AE and (b) The orthogonalized features after PCA.

VSC admittance is then generated based on thorough searching on the feature space of the training set. To take more possible impedance profiles into consideration, the upper and lower limit of each feature value are extended by 1.5 times and 20 values are evenly assigned for each feature, leading to 400 combinations. The inverse-PCA and decoding network in Fig. 3 are then applied to generate the admittances based on each feature combination. Stability of the VSC can then be evaluated based on the generated admittances and any given $L_{\rm g}$.

IV. STABILITY BOUNDARY DEVIATION AND VALIDATIONS

A. Stability Boundary Deviation

The stability boundary can then be derived. For each predicted admittance, GNC is conducted for stability analysis. Each predicted admittance is then plotted in a same figure, with unstable cases in red and stable cases in grey as Fig. 6.

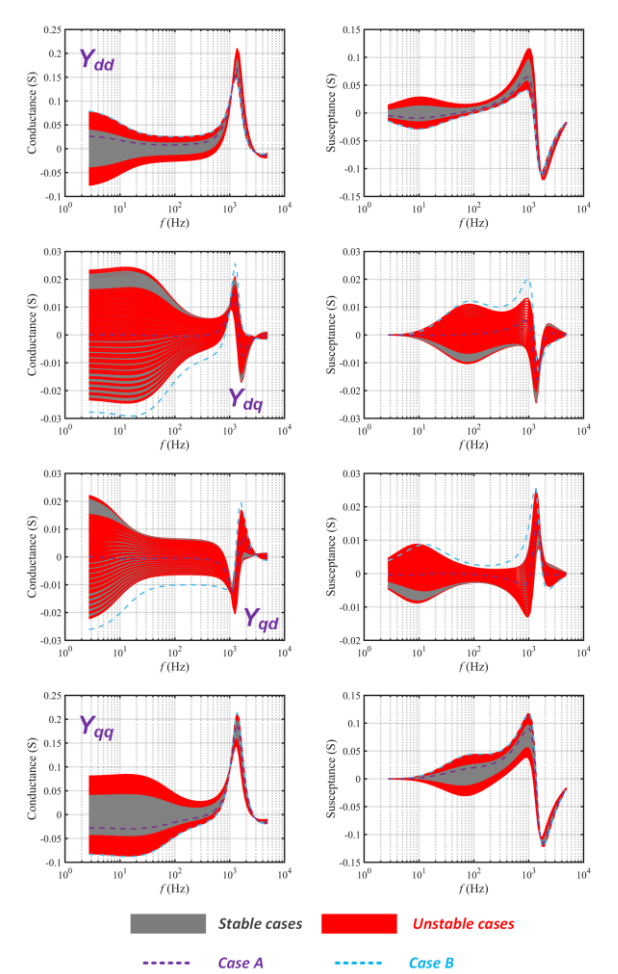


Fig. 6. Derived stability boundary.

It is shown that although the training of stacked AE and PCA only uses data from stable operating points, impedance profiles for unstable cases of the studied VSC are also successfully predicted by the proposed method. The real and imaginary part of Y_{dd} and Y_{qq} proves to be useful stability indicators, and a stability boundary can be observed. This will lead to convenient stability judgement in future applications, as the measurements of Y_{dd} and Y_{qq} at certain frequency will be sufficient for preliminary evaluation of system stability based on the derived boundary, substituting

traditional frequency scanning. Furthermore, under different grid conditions, the generated admittance profiles will not change. Therefore, a new stability boundary is easy to generate for the stability evaluation.

B. Simulation and Experiment Validations

Simulations in PLECS have been conducted to validate the proposed methodology. The parameters of the VSC are set the same as in the Appendix B. Two typical cases of operating point variation have been selected as follows. Case A: $V_{pcc} = 110 \text{ V}$, P = 1000 W, Q = 0; Case B: $V_{pcc} = 110 \text{ V}$, P = 3000 W, Q = -1500 var. The simulation results when the operating point of the VSC changes from Case A to Case B at 0.25 s are presented in Fig. 7. It is shown that instability appears in Case B, which is consistent with the derived stability boundary in Fig. 6.

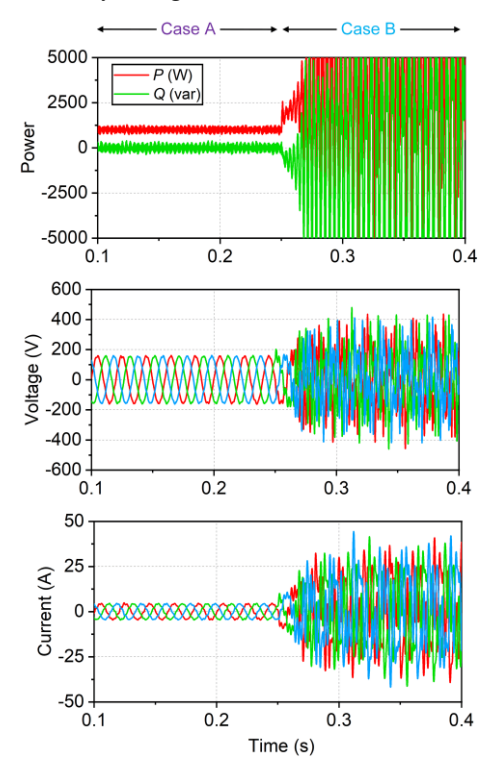


Fig. 7. Simulation results.

Experiments are also conducted to validate the proposed method. The experimental setup is shown in Fig. 8. dSPACE-1007 is used to control the VSC. The current and voltage at the PCC point is collected by current and voltage sensors and transmitted to the controller through DS2004 A/D board. The DS2102 D/A board is used to transmit the calculated power and measurements to the oscilloscope. Grid simulator Chroma 61845 is used to simulate the power grid.

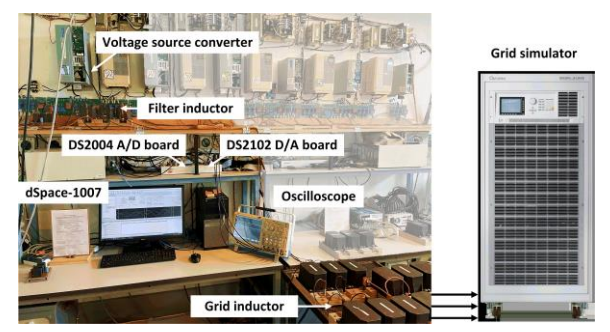


Fig. 8. Experiment setup.

The same predicted cases are selected and validated by experiments. The experiment results are shown in Fig. 6, which are consistent with the stability evaluations and simulation results.

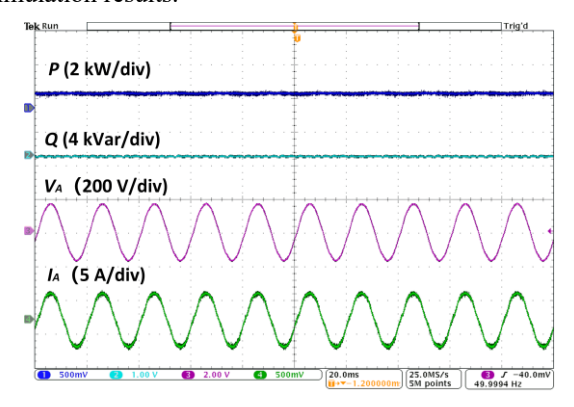


Fig. 9. Experiment result of Case A.

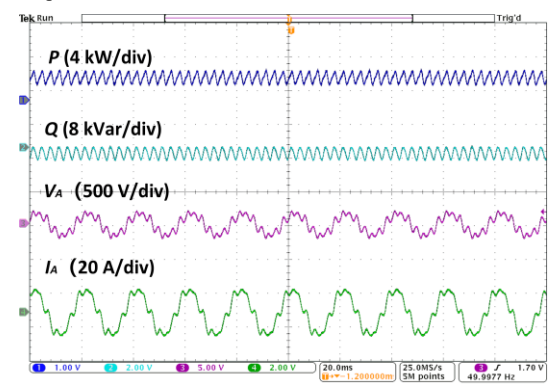


Fig. 10. Experiment result of Case B.

V. CONCLUSION

This paper has proposed a novel VSC impedance profile prediction method with unknown controller structure and parameters, solely based on collected admittance data under limited amount of stable operating points. Stacked autoencoder and PCA have been used to extract admittance feature of VSCs, and through searching on an enlarged feature space can predict impedance profiles effectively even for unstable cases. Simulation and experiment results have validated the proposed method. The proposed method will serve as an effective tool to derive the stable operation boundary for grid-connected VSCs without prior knowledge of the controller structure and parameters.

APPENDIX

APPENDIX. A

The expression of remaining transfer function matrices in the block diagram are presented as below.

$$\mathbf{G}_{PQ} = \begin{bmatrix} k_{ps} + \frac{k_{is}}{s} & 0\\ 0 & -\left(k_{ps} + \frac{k_{is}}{s}\right) \end{bmatrix}$$
(A.1)

$$\mathbf{G}_{CI} = \begin{bmatrix} k_{pi} + \frac{k_{ii}}{s} & 0\\ 0 & k_{pi} + \frac{k_{ii}}{s} \end{bmatrix}$$
(A.2)

$$\mathbf{G}_{FF} = \begin{bmatrix} 1 & 0 \\ 0 & 1 \end{bmatrix} \tag{A.3}$$

$$\mathbf{G}_{DEL} = \begin{bmatrix} \frac{1 - 0.5sT_{d}}{1 + 0.5sT_{d}} & 0\\ 0 & \frac{1 - 0.5sT_{d}}{1 + 0.5sT_{d}} \end{bmatrix}$$
(A.4)

$$\mathbf{G}_{id} = \frac{V_{dc}}{\left(sL_f + R_f\right)^2 + \left(\omega_0 L_f\right)^2} \begin{bmatrix} sL_f + R_f & \omega_0 L_f \\ -\omega_0 L_f & sL_f + R_f \end{bmatrix} \quad (A.5)$$

$$\mathbf{Z}_{f} = \begin{bmatrix} sL_{f} + R_{f} & \omega_{0}L_{f} \\ -\omega_{0}L_{f} & sL_{f} + R_{f} \end{bmatrix}$$
(A.6)

APPENDIX. B

TABLE II - PARAMETERS OF THE GRID-CONNECTED VSC

Parameter	Value	Parameter	Value
L_f	2 mH	$L_{\rm g}$	6 mH
$K_{p ext{-}PLL}$	8	K_{pi}	3
K_{i-PLL}	100	K_{ii}	10
K_{ps}	0.002	$V_{ m dc}$	600 V
Kis	0.4	$T_{ m d}$	1.5×10 ⁻⁴ s

REFERENCES

- [1] X. Wang and F. Blaabjerg, "Harmonic Stability in Power Electronic-Based Power Systems: Concept, Modeling, and Analysis," *IEEE Trans. Smart Grid*, vol. 10, no. 3, pp. 2858-2870, May 2019.
- [2] Y. Cheng, L. Fan, J. Rose, S. Huang, J. Schmall, X. Wang, etc. "Real-World Subsychronous Oscillation Events in Power Grids With High Penetrations on Inverters-Based Resources," *IEEE Trans. Power Syst.*, vol. 38, no. 1, pp. 316-330, Jan. 2023.
- [3] L. Xiong, X. Liu, Y. Liu and F. Zhuo, "Modeling and Stability Issues of Voltage-Source Converter-Dominated Power Systems: A Review," *CSEE Journal of Power and Energy Systems*, vol. 8, no. 6, pp. 1530-1549, Nov. 2020.
- [4] J. Fang, H. Deng, N. Tashakor, F. Blaabjerg and S. M. Goetz, "State-Space Modeling and Control of Grid-Tied Power Converters with Capacitive/Battery Energy Storage and Grid-Supportive Services," *IEEE J. Emerg. Sel. Topics Power Electron.*, vol. 11, no. 1, pp. 234-250, Feb. 2023.
- [5] Y. Liao, Y. Li, M. Chen, L. Nordström, X. Wang, P. Mittal and H. V. Poor, "Neural Network Design for Impedance Modeling of Power Electronic Systems Based on Latent Features," *IEEE Trans. Neural Netw. Learn. Syst.*, Early Access.
- [6] Y. Li, Y. Liao, X. Wang, L. Nordstörm, P. Mittal, M. Chen and H. V. Poor, "Neural Network Models and Transfer Learning for Impedance Modeling of Gird-Tied Inverters," in *IEEE PEDG*, Conference, 2022.
- [7] B. Wen, D. Boroyevich, R. Burgos, P. Mattavelli and Z. Shen, "Inverse Nyquist Stability Criterion for Grid-Tied Inverters," *IEEE Trans. Power Electron.*, vol. 32, no. 2, pp. 1548-1556, Feb. 2017.

- [8] B. Wen, D. Boroyevich, R. Burgos, P. Mattavelli and Z. Shen, "Inverse Nyquist Stability Criterion for Grid-Tied Inverters," *IEEE Trans. Power Electron.*, vol. 32, no. 2, pp. 1548-1556, Feb. 2017.
- [9] A. Frances, D. Ramirez and J. Uceda, "Blackbbox Small-Signal Modeling of Grid-Connected Inverters in Asymmetrical Power Grids," *IEEE Trans. Power Electron.*, vol. 38, no. 10, pp. 13064-13073, Oct. 2023.
- [10] H. Gong. X. Wang and D. Yang, "DQ-Frame Impedance Measurement of Three-Phase Converters Using Time-Domain MIMO Parametric Identification," *IEEE Trans. Power Electron.*, vol. 36, no. 2, pp. 2131-2142, Feb. 2021.
- [11] S. FØyen, C. Zhang, Y. Zhang, T. Isobe, O. B. Fosso, X. Cai and M. Molinas, "Frequency Scanning of Weakly Damped Single-Phase

- VSCs With Chirp Error Control," *IEEE Trans. Power Electron.*, vol. 38, no. 9, pp. 10692-10701, May 2023.
- [12] W. Liu, X. Xie, J. Shair and J. Zhang, "Stability Region Analysis of Grid-Tied Voltage Sourced Converters Using Variable Operating Point Impedance Model," *IEEE Trans. Power Syst.*, vol. 38, no. 2, pp. 1125-1137, Mar. 2023.
- [13] Y. Wu, P. Zhang and G. Lu, "Detection and Location of Aged Cable Segment in Underground Power Distribution System Using Deep Learning Approach," *IEEE Trans. Ind. Informat.*, Vol. 17, no. 11, pp. 7379-7389, Nov. 2021
- [14] Y. Wu, Y. Yang, Z. Wang and P. Zhang, "Online Monitoring for Underground Power Cable Insulation Based on Common-Mode Signal Injection," *IEEE Trans. Ind. Electron.*, vol. 69, no. 7, pp. 7360-7371, Jul. 2022.